Int. J. Heat Mass Transfer. Vol. 31, No. 11, pp. 2331–2338, 1988
Printed in Great Britain

0017–9310/88 $3.00 + 0.00
Pergamon Press plc

Numerical study of steady-state laser melting problem

BISWAJIT BASU
Tata Research Development and Design Centre, 1, Mangaldas Road, Pune 411 001, India

and

J. SRINIVASAN
Indian Institute of Science, Bangalore 560 012, India

(*Received* 24 *June* 1987 *and in final form* 10 *February* 1988)

Abstract—A two-dimensional steady-state laser melting problem is numerically simulated. A vorticity–stream function formulation is used to solve momentum equations and a method of selecting the optimum relaxation parameter is suggested. Steady-state finite-difference equations are solved by an alternative direction implicit (ADI) scheme using a false transient formulation. A solid and liquid interface is approximated by steps. The role of surface tension driven flow on total heat transfer is studied. Comparative studies are carried out between conduction and convection results. The flow pattern in the molten pool is presented through stream function plots which show the effect of laser power on the size and strength of secondary cells. The effect of a secondary cell on the total heat transfer and pool shape is analysed under varying laser power.

1. INTRODUCTION

LASER melting and solidification has received a lot of attention recently due to the improved surface properties that can be achieved [1]. Due to rapid solidification soon after the melting better surface properties can be obtained, especially from the point of view of wear and corrosion resistances. Moreover, the penetration depth, i.e. the depth of the molten pool, is small during laser surface treatment because of the small time of interaction. This is of great importance from the manufacturing point of view where one wants to retain the bulk properties of the product the same with a thin surface of special properties. Its potential has, however, not yet been fully utilized. The primary reason is that the basic mechanism governing the process has not been fully understood. Anthony and Cline [2] did the first quantitative work and proposed that the flow in the melt was created by the surface tension gradient at the free surface. They assumed the flow field was not coupled to the heat transfer and studied a one-dimensional model. Hence, they did not study the effect of the flow on heat transfer.

Chan *et al.* [3] considered a two-dimensional transient model of laser melting. Movement of the heat source was taken into consideration by coordinate transformation. On the basis of wrong values of latent heat of fusion, they neglected the interface energy balance because of the low value of latent heat of fusion. Quantitative effects of different parameters on the surface velocity, surface temperature, pool shape and cooling rate were presented. Chan *et al.*'s work [3], however, clearly shows the effect of fluid flow on the total heat transfer during laser melting. In the subsequent work, Chan *et al.* [4] analysed a steady-state laser melting problem with a stationary beam in the cylindrical coordinate system. They validated their model by comparing experimental results to that obtained from the model. They found that scanning velocity plays an insignificant role because of the higher magnitude of the surface tension velocity. Later, this fact was proved in ref. [5] while analysing thermocapillary flow during laser melting. Chan *et al.* [6] analysed laser surface alloying at different cross-sections along the workpiece.

In all the previous studies [3, 4, 6], a detailed analysis of the flow in the pool was not carried out. The effect of the flow on the total heat transfer was the main consideration of all those studies. In this paper, a steady-state analysis of the laser melting problem is presented. The changes of flow pattern with the increasing power of the beam is shown clearly. The role of the secondary cell on the heat transfer and, subsequently, on the pool shape is analysed.

2. DEFINITION OF THE PROBLEM

To develop a mathematical model, the problem is physically defined as follows. A laser beam having a constant power distribution strikes the surface of the material. All of the incident radiation is assumed to be absorbed by the material. The heat absorbed develops a molten pool. The flow is produced mainly due to the surface tension gradient [6]. The surface tension gradient is produced by the temperature gradi-

NOMENCLATURE

d	height of the workpiece [m]
k	thermal conductivity [$W m^{-1} K^{-1}$]
Ma	Marangoni number, $(d\sigma/dT^*)(qr_0/k)(r_0/\mu\alpha)$
P	pressure [$N m^{-2}$]
q	input heat flux [$W m^{-2}$]
R_σ	surface tension Reynolds number, $(d\sigma/dT^*)(qr_0/k)(r_0/\mu\nu)$
r_0	width of the laser beam [m]
T	temperature [K]
U_c	characteristic surface tension velocity $(d\sigma/dT^*)(qr_0/k\mu)$ [$m s^{-1}$]
u	vertical velocity
v	horizontal velocity
W	any independent variable
x	vertical coordinate
y	horizontal coordinate.

Greek symbols

α	thermal diffusivity [$m s^{-2}$]
ε	convergence criteria
μ	dynamic viscosity [$N m^{-1} s^{-1}$]
ν	kinematic viscosity [$m s^{-2}$]
ρ	density [$kg m^{-3}$]
σ	surface tension [$N m^{-1}$]
$\Delta\tau$	false time step or relaxation parameter
ψ	stream function
Ω	vorticity.

Subscripts

a	ambient
c	characteristic value
l	liquid
liq	point where the interface intersects a reference line
m	melting point
s	solid
w	wall or interface.

Superscript

*	dimensional value.

ent at the free surface. The surface tension gradient acts as a shear stress at the surface itself and, thus, induces convective flows. The problem is to determine the flow pattern, pool shape, free surface temperature and velocity distribution at the steady state with the increasing power of the beam. The model is shown in Fig. 1.

The following assumptions are made for the present model.

(1) The heat conduction and fluid flow are primarily in the x- and y-directions. Conduction and convection in the z-direction is neglected. This assumption is reasonable because of the symmetry of the problem.

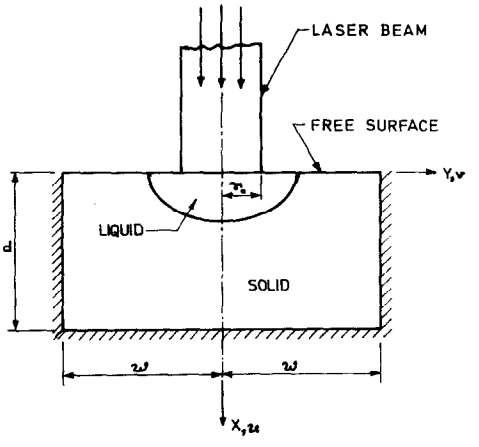

FIG. 1. Coordinate system.

(2) All properties of the material are independent of temperature except surface tension.

(3) The surface of the melt is flat. This assumption was justified in ref. [5].

(4) The laser beam is stationary. Though the laser melting process is a moving heat source problem, ref. [5] has shown that the quasi-steady-state analysis is valid to study the flow pattern.

(5) The free surface outside the beam is adiabatic.

(6) The heat flux at the boundary represents the net heat input to the material.

3. MATHEMATICAL FORMULATION

Using the symmetry, the present problem can be mathematically defined by the following governing equations and boundary conditions.

For liquid region

Energy equation

$$u^* \frac{\partial T^*}{\partial x^*} + v^* \frac{\partial T^*}{\partial y^*} = \alpha_l \left(\frac{\partial^2 T^*}{\partial x^{*2}} + \frac{\partial^2 T^*}{\partial y^{*2}} \right). \quad (1)$$

Momentum equations

$$u^* \frac{\partial u^*}{\partial x^*} + v^* \frac{\partial u^*}{\partial y^*} = -\frac{1}{\rho} \frac{\partial p^*}{\partial x^*} + \nu \left(\frac{\partial^2 u^*}{\partial x^{*2}} + \frac{\partial^2 u^*}{\partial y^{*2}} \right) \quad (2)$$

$$u^* \frac{\partial v^*}{\partial x^*} + v^* \frac{\partial v^*}{\partial y^*} = -\frac{1}{\rho} \frac{\partial p^*}{\partial y^*} + \nu \left(\frac{\partial^2 v^*}{\partial x^{*2}} + \frac{\partial^2 v^*}{\partial y^{*2}} \right). \quad (3)$$

Continuity equation

$$\frac{\partial u^*}{\partial x^*} + \frac{\partial v^*}{\partial y^*} = 0. \tag{4}$$

For solid region

Energy equation

$$\frac{\partial^2 T^*}{\partial x^{*2}} + \frac{\partial^2 T^*}{\partial y^{*2}} = 0. \tag{5}$$

The boundary conditions are as follows:

$$\left.\begin{aligned}
&\text{at } x^* = 0,\\
&\quad -k\frac{\partial T^*}{\partial x^*} = q; && 0 \leqslant y^* \leqslant r_0\\
&\qquad\quad = 0; && r_0 < y^* \leqslant w\\
&\quad u^* = 0,\ \mu\frac{\partial v^*}{\partial x^*} = -\frac{\partial \sigma}{\partial y^*}; && 0 \leqslant y^* \leqslant y_{\text{liq}}\\
&\text{at } y^* = 0,\\
&\quad v^* = \frac{\partial u^*}{\partial y^*} = \frac{\partial T^*}{\partial y^*} = 0; && 0 \leqslant x^* \leqslant d\\
&\text{at the interface, } u^* = v^* = 0 \text{ and } T^* = T_{\text{m}}^*\\
&\text{at } x^* = d, \quad T^* = T_{\text{a}}^*; \quad 0 \leqslant y^* \leqslant w\\
&\text{at } y^* = w, \quad T^* = T_{\text{a}}^*; \quad 0 \leqslant x^* \leqslant d.
\end{aligned}\right\} \tag{6}$$

The initial condition is

$$T^* = T_{\text{a}}^*; \quad 0 \leqslant x^* \leqslant d \text{ and } 0 \leqslant y^* \leqslant w. \tag{7}$$

The solid–liquid interface is determined by the melting point temperature and no energy balance is required at the interface because of steady-state analysis. The governing equations are nondimensionalized with the following non-dimensional variables:

$$x = \frac{x^*}{r_0}; \quad y = \frac{y}{r_0}; \qquad T = \frac{T^* - T_{\text{a}}^*}{(qr_0/k)}$$

$$u = \frac{u^*}{U_{\text{c}}}; \quad v = \frac{v^*}{U_{\text{c}}} \quad \text{and} \quad p = \frac{p^*}{\rho U_{\text{c}}^2}.$$

The characteristic surface tension velocity, U_{c}, can be obtained from the order analysis of the free surface force balance between the surface tension and shear forces [5], and can be expressed as follows:

$$U_{\text{c}} = \frac{\mathrm{d}\sigma}{\mathrm{d}T^*}\frac{qr_0}{k\mu}.$$

Introducing the dimensionless variables and transforming the momentum equations to the 'vorticity transport equation' (i.e. to eliminate the pressure gradient terms), the complete mathematical description of the problem is as follows.

For liquid region

Energy equation

$$u\frac{\partial T}{\partial x} + v\frac{\partial T}{\partial y} = \frac{1}{Ma}\left(\frac{\partial^2 T}{\partial x^2} + \frac{\partial^2 T}{\partial y^2}\right). \tag{8}$$

Vorticity transport equation

$$u\frac{\partial \Omega}{\partial x} + v\frac{\partial \Omega}{\partial y} = \frac{1}{R_\sigma}\left(\frac{\partial^2 \Omega}{\partial x^2} + \frac{\partial^2 \Omega}{\partial y^2}\right). \tag{9}$$

Stream function equation

$$\Omega = -\left(\frac{\partial^2 \psi}{\partial x^2} + \frac{\partial^2 \psi}{\partial y^2}\right). \tag{10}$$

Velocities

$$u = \frac{\partial \psi}{\partial y} \quad \text{and} \quad v = -\frac{\partial \psi}{\partial x}. \tag{11}$$

The boundary conditions are as follows:

$$\left.\begin{aligned}
&\text{at } x = 0,\\
&\quad -\frac{\partial T}{\partial x} = 1.0; && 0 \leqslant y \leqslant 1.0\\
&\qquad\quad = 0; && 1.0 < y \leqslant \frac{w}{r_0}\\
&\quad u = 0; && 0 \leqslant y \leqslant y_{\text{liq}}\\
&\quad \frac{\partial v}{\partial x} = -\frac{\partial T}{\partial y}; && 0 \leqslant y \leqslant y_{\text{liq}}\\
&\text{at } y = 0,\\
&\quad v = \frac{\partial u}{\partial y} = \frac{\partial T}{\partial y} = 0; && 0 \leqslant x \leqslant \frac{d}{r_0}\\
&\text{at the interface, } u = v = 0 \text{ and } T = T_{\text{m}}.
\end{aligned}\right\} \tag{12}$$

The vorticity at the free surface is determined using boundary conditions (12) and the definition of vorticity

$$\Omega|_{x=0} = \frac{\partial T}{\partial x}. \tag{13}$$

Along the line of symmetry

$$\frac{\partial \Omega}{\partial y} = 0. \tag{14}$$

The interface vorticity is determined by assuming the interface as a no-slip wall and, therefore, the interface vorticity is determined as follows [7]:

$$\Omega = -\frac{2\psi_{w+1}}{\Delta w^2}. \tag{15}$$

Since there is no flow across the system boundary, the stream function boundary conditions are

$$\left.\begin{aligned}
&\text{at } x = 0, \ \psi = 0; \quad 0 \leqslant y \leqslant y_{\text{liq}}\\
&\text{at } y = 0, \ \psi = 0; \quad 0 \leqslant x \leqslant x_{\text{liq}}\\
&\text{at the interface, } \psi = 0.
\end{aligned}\right\} \tag{16}$$

For solid region

Energy equation

$$\frac{\partial^2 T}{\partial x^2} + \frac{\partial^2 T}{\partial y^2} = 0. \tag{17}$$

The boundary conditions are as follows:

$$\left.\begin{aligned} &\text{at } x = 0, \quad \frac{\partial T}{\partial x} = 0; \quad y_{\text{liq}} < y \leqslant \frac{w}{r_0} \\ &\text{at } x = \frac{d}{r_0}, \quad T = 0; \quad 0 \leqslant y \leqslant \frac{w}{r_0} \\ &\text{at } y = 0, \quad \frac{\partial T}{\partial y} = 0; \quad x_{\text{liq}} < x \leqslant \frac{d}{r_0} \\ &\text{at } y = \frac{w}{r_0}, \quad T = 0; \quad 0 \leqslant x \leqslant \frac{d}{r_0} \end{aligned}\right\} \tag{18}$$

at the interface, $T = T_m$.

The initial condition is

$$T = 0; \quad 0 \leqslant x \leqslant \frac{d}{r_0} \text{ and } 0 \leqslant y \leqslant \frac{w}{r_0}. \tag{19}$$

4. NUMERICAL DESCRIPTION

The finite-difference form of equations (9)–(11) along with the boundary conditions, i.e. equations (12)–(16), for the liquid region and equation (17) along with the boundary conditions, i.e. equation (18), are solved by the ADI method. The steady-state problem is solved by the false transient method.

To start the solution, the pure conduction equation has to be solved till a certain molten pool region is created so that the momentum (i.e. vorticity transport) equation can be applied. For the present study, the vorticity transport equation is solved when there are 30 grids in the molten region. Because of a very high Reynolds number, a second-order upwind differencing scheme is used to evaluate the convective terms of the energy and vorticity equations [6]. The diffusion terms of both the energy and vorticity equations are evaluated by the central differencing scheme.

The solid–liquid interface is approximated by steps and it is clearly shown in Fig. 2. The interface is tracked by the melting point temperature. Since there is no role of latent heat of fusion in the steady-state problem, a grid point is termed as the interface as soon as the temperature of that grid point reaches the melting point without any energy balance at that grid point, i.e. across the solid–liquid interface. For the present study (41 × 41) grids are used with step sizes of 0.1 in both the X- and Y-directions.

4.1. *Selection of relaxation parameter (false time step)*

The selection of the relaxation parameter is one of the most important aspects in any steady-state numerical problem. The relaxation parameters or false time steps of the present problem in both the regions are determined on the basis of the dominant

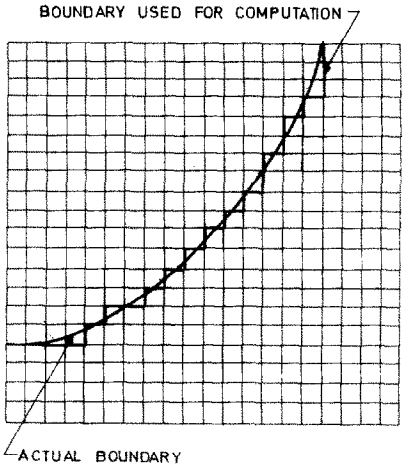

FIG. 2. Numerical approximation of the actual interface.

governing mechanism. In the solid region, thermal diffusion is the mode of heat transfer and, hence, the false time step is defined on the basis of thermal diffusion velocity (α_s/r_0). On the other hand, convection is the dominant mode of heat transfer in the liquid region and the characteristic surface tension velocity (U_c) is used to define the false time step. The false time steps in the solid and liquid are selected in such a manner that both of them should represent the same physical time. On this basis, the relation between false time steps in the solid and liquid regions is

$$\frac{\Delta\tau_l}{\Delta\tau_s} = Ma\left(\frac{\alpha_l}{\alpha_s}\right). \tag{20}$$

The relative error (i.e. fractional change) criterion is used to ascertain whether steady state is reached or not. This criterion is defined as

$$\left|\frac{W^{\text{new}} - W^{\text{old}}}{W^{\text{old}}}\right| < \varepsilon; \quad W^{\text{old}} \neq 0 \tag{21}$$

where W is any dependent variable and ε is a small quantity. For the present study the value of ε is selected as 0.005.

4.2. *Selection of governing parameters*

From the non-dimensional forms of the governing equations (equations (9)–(11)), the non-dimensional parameters, governing the present problem, are identified as follows:

R_σ = Surface tension Reynolds number

$$= \frac{\mathrm{d}\sigma}{\mathrm{d}T^*}\frac{qr_0}{k}\frac{r_0}{\mu\nu}$$

Ma = Marangoni number

$$= \frac{\mathrm{d}\sigma}{\mathrm{d}T^*}\frac{qr_0}{k}\frac{r_0}{\mu\alpha}$$

T_m = Non-dimensional melting point.

The results are obtained for the following three cases.

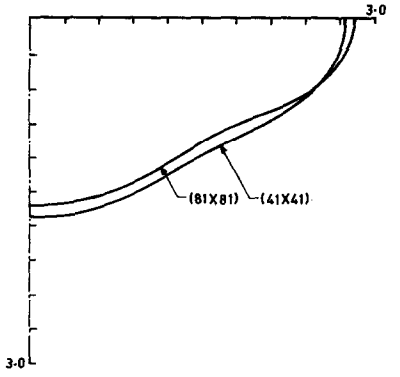

FIG. 3. Comparison of pool shapes with (41 × 41) and (81 × 81) grids for $R_\sigma = 20\,000.0$, $Ma = 2000.0$ and $T_m = 0.125$.

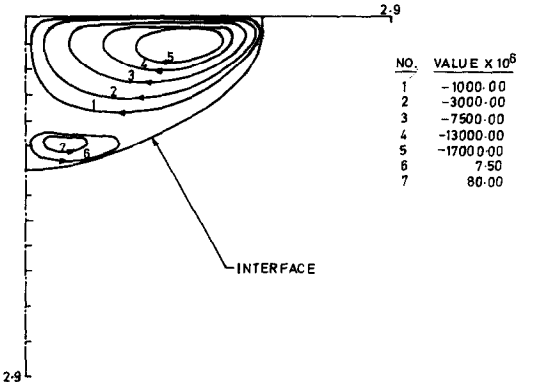

FIG. 4. Streamlines in the molten pool for $R_\sigma = 10\,000.0$, $Ma = 1000.0$ and $T_m = 0.25$.

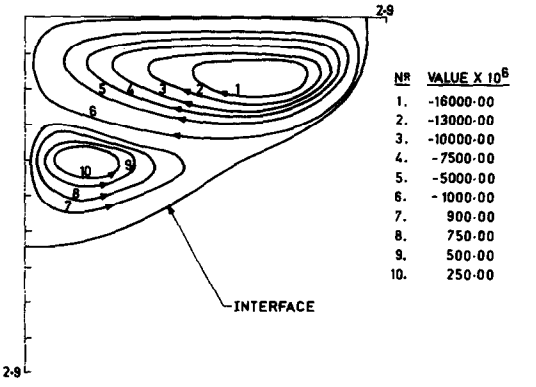

FIG. 5. Streamlines in the molten pool for $R_\sigma = 20\,000.0$, $Ma = 2000.0$ and $T_m = 0.125$.

Case I: $Ma = 1000.0$

$R_\sigma = 10\,000.0$

$T_m = 0.25$.

Case II: $Ma = 2000.0$

$R_\sigma = 20\,000.0$

$T_m = 0.125$.

Case III: $T_m = 0.25$ (pure conduction).

For steel, different cases represent the following physical values.

Cases I and III: $q = 2.7 \times 10^8$ W m^{-2}

$r_0 = 1.0$ mm.

Case II: $q = 5.4 \times 10^8$ W m^{-2}

$r = 1.0$ mm.

The values of one relaxation parameter (i.e. false time step), for the solid zone, are

Cases I and III = 0.008

Case II = 0.004.

The number of iterations required to reach the steady-state solution for different cases are

Case I = 835

Case II = 1300

Case III = 275.

The number of iterations is highest in case II because the value of the relaxation parameter is smallest in this case. To study the effect of the grid size on the solution, pool shapes for case II with (41 × 41) and (81 × 81) grids are compared and shown in Fig. 3. The grid sizes are 0.1 and 0.05 for (41 × 41) and (81 × 81) grids, respectively. From Fig. 3 it can be seen that the pool shapes are within reasonable accuracy.

5. RESULTS AND DISCUSSION

The streamlines for different cases (i.e. cases I and II) are shown in Figs. 4 and 5. From the streamline plots, it can be seen that there is a secondary cell at the bottom of the molten pool. The size and strength of this cell are larger for $R_\sigma = 20\,000.0$ than for $R_\sigma = 10\,000.0$. Reference [5] observed the existence of these cells during an analysis of the thermocapillary flow in a rectangular cavity. In a rectangular cavity secondary cells form because of the corner effect while secondary cells exist in the molten pool due to its flat shape. The fluid cannot take a sharp turn near the bottom of the pool because of its flat shape which results in the formation of secondary cells. As can be seen from Figs. 4 and 5, the point of deviation of the bulk flow from the interface is different for these two cases. For case II, the order of magnitude of velocity, i.e. the momentum of fluid, is higher than that of case I because of the higher power of the beam. As a result, the bulk flow for case II deviates at a point which is at a lower depth than that for case I and, thereby, creates secondary cells of higher size and strength.

The isotherms for different cases (i.e. I, II and III) are shown in Figs. 6–8. The effect of flow on heat transfer is clearly seen from these plots. In the presence of recirculating flow, heat transfer takes place by both

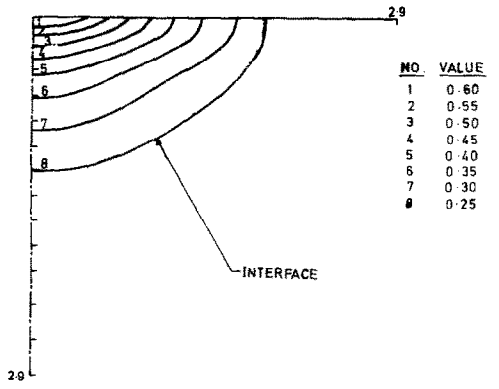

FIG. 6. Isotherms in the molten pool for $R_\sigma = 10\,000.0$, $Ma = 1000.0$ and $T_m = 0.25$.

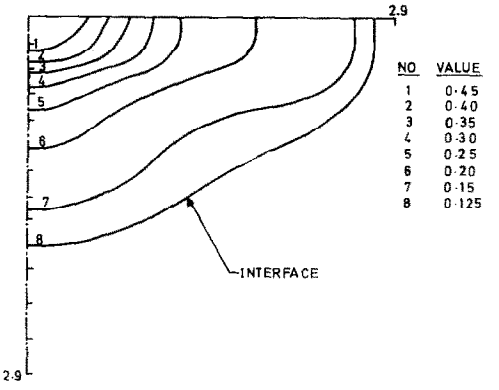

FIG. 7. Isotherms in the molten pool for $R_\sigma = 20\,000.0$, $Ma = 2000.0$ and $T_m = 0.125$.

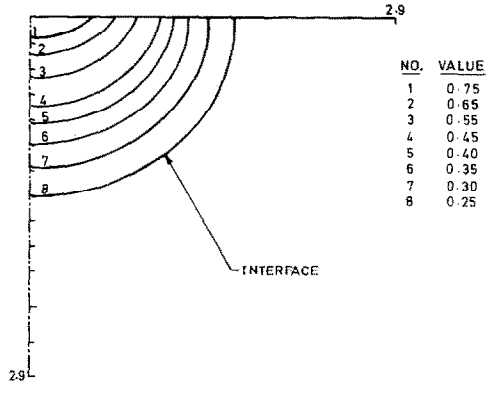

FIG. 8. Isotherms in the molten pool for $T_m = 0.25$ with pure conduction.

conduction and convection. Due to the presence of the bulk flow (i.e. primary cell), heat transfer by conduction is opposed by the convection near the line of symmetry. Away from the line of symmetry, heat transfer by convection is in the same direction as that by conduction. As a result, total heat transfer is enhanced along the Y-direction and decreased near the line of symmetry because of the bulk flow. On the other hand, secondary cells at the bottom of the melt modify the heat transfer mechanism in the opposite way and enhance the total heat transfer near the line of symmetry. For $R_\sigma = 20\,000.0$, this secondary cell modifies the total heat transfer substantially and this can be seen from the last two isotherms of Fig. 7. The aspect ratios (width/depth of the molten pool) of all the cases are given in Table 1. The aspect ratios of cases I and II are more than that of case III which is due to pure conduction. This is because of the convective heat transfer which makes the pool shallower. The aspect ratios of cases I and II are almost the same (Table 1). As Reynolds number increases, the width of the pool increases because of a higher contribution of convective heat transfer due to higher orders of magnitude of bulk flow velocity (Table 1). On the other hand, the depth of the pool, also, increases because the secondary cell of higher strength enhances the total heat transfer near the line of symmetry (Table 1). As a result, both depth and width increase as Reynolds number increases and the ratio of width to depth (i.e. aspect ratio) is almost the same for both the cases under the present study.

Table 1. Steady-state melt geometry

Case No.	Width	Depth	Aspect ratio
I	1.72	1.14	1.50
II	2.73	1.84	1.48
III	1.48	1.32	1.12

The non-dimensional free surface temperature distributions are shown in Fig. 9. The maximum temperature occurs at the centre of the beam and decreases away from the beam. The maximum surface temperature gradient occurs near the edge of the beam because of the sudden change in the boundary heat transfer. The maximum temperature of case III is more than that of cases I and II because of more heat accumulation due to the absence of convective heat transfer. The maximum temperature of case II is lower than that of case I because of better mixing in the presence of flow of a higher order of magnitude.

The velocity distribution at the free surface is shown in Fig. 10. The velocity at the centre is zero and increases away from the centre. The velocity at the free surface attains a maximum value at a point where the free surface temperature gradient is maximum, i.e. near the edge of the beam. This is because of the fact that flow is driven by the free surface temperature gradient which induces the surface tension gradient there. Although the non-dimensional velocities of case I (i.e. $R_\sigma = 10\,000.0$) are higher than that of case II (i.e. $R_\sigma = 20\,000.0$), the dimensional velocities are always higher with higher Reynolds numbers. For example, the maximum values of maximum velocities for cases I and II are 2.0 and 3.0 m s^{-1}, respectively, using steel as the material under study.

6. CONCLUSION

The convection occurring due to recirculating thermocapillary flow dominates the heat transfer process

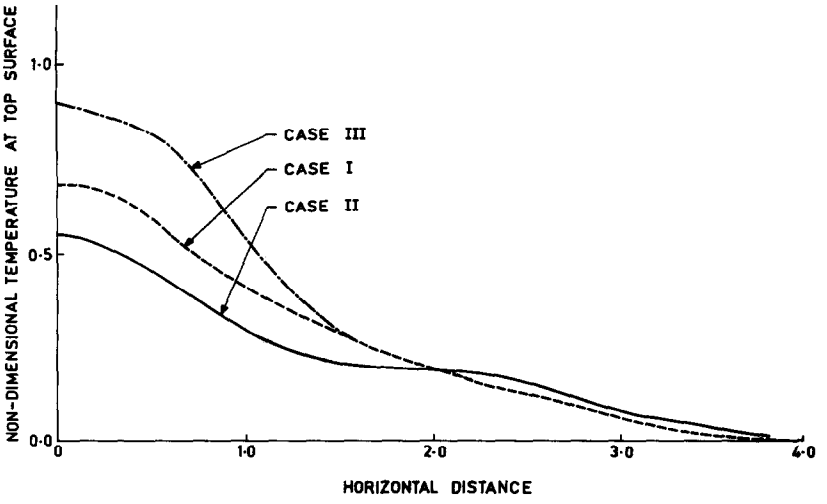

FIG. 9. Non-dimensional temperature distribution at the top surface for all cases.

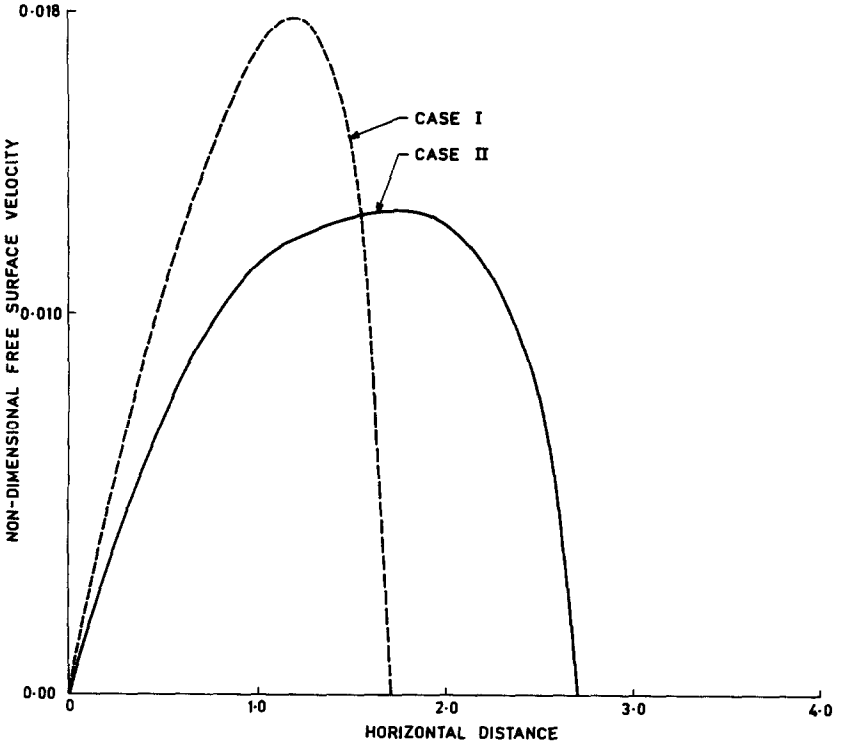

FIG. 10. Free surface velocity distribution for all cases.

during laser melting and, hence, modifies the pool shape. A secondary cell exists at the bottom of the molten pool and modifies the total heat transfer process near the line of symmetry at high Reynolds numbers, i.e. with high powered beams. As a result, there will be no significant change in the aspect ratio of the molten pool when the heat flux incident on the surface is increased.

Acknowledgements—We would like to thank Prof. E. C. Subbarao, Tata Research Development & Design Centre, Pune, and Prof. A. W. Date, Indian Institute of Technology, Bombay, for several fruitful discussions. This work was supported by a project from Defence Research Development Organization, New Delhi.

REFERENCES

1. A. Tiziani, L. Giordano and E. Ramous, Laser surface treatment by rapid solidification. In *Lasers in Materials Processing* (Edited by E. A. Metzbower), pp. 108–114. American Society for Metals (1983).
2. T. R. Anthony and H. E. Cline, Surface rippling induced

by surface tension gradients during laser surface melting and alloying, *J. Appl. Phys.* **48**(9), 3889–3894 (1977).
3. C. Chan, J. Mazumder and M. M. Chen, A two dimensional transient model for convection in laser melted pool, *Metall. Trans.* **15A**, 2175–2184 (1984).
4. C. Chan, J. Mazumder and M. M. Chen, Three dimensional model for convection in laser melted pool, presented at ICALEO (1985).
5. J. Srinivasan and B. Basu, A numerical study of thermocapillary flow in a rectangular cavity during laser melting, *Int. J. Heat Mass Transfer* **24**, 563–572 (1986).
6. C. Chan, J. Mazumder and M. M. Chen, A model for surface tension flows in laser surface alloying. In *Lasers in Material Processing* (Edited by E. A. Metzbower), pp. 150–157. American Society for Metals (1983).
7. P. J. Roach, *Computational Fluid Dynamics* (Revised Edn). Albuquerque, U.S.A. (1976).

ETUDE NUMERIQUE D'UN PROBLEME PERMANENT DE FUSION LASER

Résumé—On simule numériquement un problème bidimensionnel permanent de fusion laser. La formulation vorticité–fonction de courant est utilisée pour résoudre les équations de quantité de mouvement et on suggère une méthode de sélection du paramètre optimal de relaxation. Les équations aux différences finies sont résolues par un schéma implicite de direction alternée (ADI) qui utilise une formulation faussement transitoire. L'interface solide–liquide est approché par pas. On étudie le rôle de la tension interfaciale sur le transfert thermique global. Des études comparatives sont faites entre les résultats de conduction et de convection. La configuration d'écoulement dans le bain fondu est présentée à travers les figures de la fonction de courant, ce qui montre l'effet de la puissance laser sur la taille et l'intensité des cellules secondaires. L'effet d'une cellule secondaire sur le transfert thermique total et sur la forme du bain est analysé pour une puissance laser variable.

NUMERISCHE UNTERSUCHUNG DES STATIONÄREN LASER-SCHMELZ-VERFAHRENS

Zusammenfassung—Der zweidimensionale stationäre Laser-Schmelz-Vorgang wurde numerisch simuliert. Zur Lösung der Impulsgleichungen wurde ein Ansatz mit der Wirbelstromfunktion verwendet. Eine Methode zur Ermittlung des optimalen Relaxationsparameters wird vorgeschlagen. Die Finite-Differenzen-Gleichungen für den stationären Fall wurden mit dem impliziten Verfahren der alternierenden Richtungen (ADI) gelöst. Der Verlauf der Phasengrenze fest/flüssig wurde schrittweise berechnet. Der Einfluß der durch Oberflächenspannung hervorgerufenen Strömung auf den gesamten Wärmetransport wurde untersucht. Die Werte der Wärmeübertragung durch Wärmeleitung und Konvektion wurden verglichen. Mit Bildern des Strömungspotentials wurden die Strömungsmuster im Schmelzbad dargestellt. Dadurch wird die Auswirkung der Laserleistung auf die Größe und Stärke von sekundären Zellen gezeigt. Der Einfluß eines sekundären Wirbels auf den Gesamtwärmeübergang und die Form des Schmelzbades wurde unter Veränderung der Laserleistung untersucht.

ЧИСЛЕННОЕ ИССЛЕДОВАНИЕ СТАЦИОНАРНОЙ ЗАДАЧИ ЛАЗЕРНОЙ ПЛАВКИ

Аннотация—Проведено численное моделирование двухмерной стационарной задачи лазерной плавки. Уравнения количества движения решаются с применением соотношения между завихренностью и функцией тока. Предложен метод выбора оптимального параметра релаксации. Стационарные конечноразностные уравнения решаются с использованием неявной схемы переменных направлений. Проводится ступенчатая аппроксимация поверхности раздела между твердым телом и жидкостью. Изучается влияние вызванного поверхностным натяжением течения на процесс теплопереноса. Проведен сравнительный анализ результатов по теплопроводности и конвекции. Картина течения в объеме расплава представлена в виде графиков для функции тока, отражающих влияние мощности лазера на размер и интенсивность вторичных ячеек. Анализируется влияние вторичной ячейки на суммарный теплоперенос и форму расплава.